# Effect of Ag Adatoms on High-Coverage Alkanethiolate Adsorption on Au(111)

**M. H. Fonticelli,[‡] G. Benítez,[‡] P. Carro,[†] O. Azzaroni,[‡] R. C. Salvarezza,[‡] S. Gonzalez,[§] D. Torres,[§] and F. Illas*[,§]**

*Departamento de Química Física, Universidad de La Laguna, Tenerife, Spain, Instituto de Investigaciones Fisicoquímicas Teóricas y Aplicadas (INIFTA), Universidad Nacional de La Plata, CONICET, Sucursal 4 Casilla de Correo 16 (1900) La Plata, Argentina, and Departament de Química Física and ITQCUB, Universitat de Barcelona and PCB, E-08028 Barcelona, Spain*

*Received: June 18, 2007; In Final Form: October 9, 2007*

Alkanethiol adsorption on Ag-adatom-modified Au(111) surfaces is studied by means of electrochemical techniques combined with Auger electron spectroscopy and periodic density functional (DF) calculations. The bimetallic surfaces are prepared by Ag underpotential deposition, and only the alkanethiolate high-coverage regime is considered. Alkanethiolate electrodesorption from Ag-modified Au(111) surfaces requires potentials shifted 0.3 eV in the negative direction with respect to the value corresponding to desorption from Au(111) surfaces. In agreement with this experimental result, DF calculations show that alkanethiolates prefer to be laterally adsorbed to Ag adatoms, the interaction energy being 0.3 eV larger than that corresponding to the same thiolate on Au(111). Therefore, it is concluded that alkanethiolates adsorbed on Au are likely to be observed only when the Ag adatom surface density is small enough or all Ag sites are occupied. The preference for alkanethiolate adsorption on adatoms is also found for a model surface containing Au adatoms on Au(111). This indicates that no significant differences in electrodesorption potentials should be expected between Ag-adatom- and Au-adatom-rich surfaces. These findings and the analysis of experimental results strongly suggest that, under experimental conditions, the Au(111) surface does not exhibit a significant amount of Au adatoms, thus casting reasonable doubts on the adatom reconstruction models proposed for thiolates on Au(111).

## Introduction

Alkanethiolate self-assembled monolayers (SAMs) on metals, particularly Cu, Ag, and Au, have attracted considerable scientific and technological attention because they provide a route to control corrosion, wetting, and wear properties of metal surfaces.[1] SAMs serve also to anchor different functional groups employed as chemical and biochemical sensors.[2,3] They are also useful for pattern transfer in microcontact printing, to carry out dip pen lithography,[4] to fabricate nanodevices for electronics,[5,6] constitute promising candidates for new nanofabrication methods,[7] and, finally, provide ideal model systems for interface science.[8]

The adsorption of alkanethiolates on Au(111) from ethanolic solutions or from the gas phase leads to dense and ordered structures such as Au(111)-($\sqrt{3} \times \sqrt{3}$)R30° and Au(111)-c(4 × 2).[2,9] The nature of alkanethiolate adsorption sites on Au(111) is still under debate, particularly concerning the comparison between experimental results and theoretical predictions from density functional (DF) calculations.[10−17] Recently, scanning tunneling microscopy (STM) imaging and DF calculations suggested that Au adatoms on Au(111), produced during the lifting of the Au(111)-(22 × $\sqrt{3}$) surface reconstruction, play a relevant role in the formation of the stripe alkanethiolate phase formed at low Au adatom surface coverage.[18] The important role of Au adatoms is evidenced in recent DF calculations[17] suggesting that the dense phases of vertically placed alkanethiolates on Au(111) consist also of species bonded to Au adatoms produced in a massive surface reconstruction process. However, the influence of Au adatoms on the alkanethiolate adsorption at high coverage has not been experimentally explored. In particular, it is very difficult to produce a controlled amount of Au adatoms and also to determine their position on the Au surface.

A possible way to circumvent the problems described above, arising from the indistinct chemical nature of atoms in the adlayer and in the underlying substrate, is to use a second metal which could be deposited in a controlled way even at a high-coverage regime. In this work we follow this strategy to study alkanethiol adsorption on a Au(111) surface modified by underpotential deposition (UPD) of Ag adatoms. UPD allows a precise control of the amount of Ag adatoms. Therefore, the influence of adatom coverage on thiol adsorption properties can be investigated in a straightforward way. Here, this is done by inspecting electrodesorption curves of propanethiolate (PT) SAMs on Ag-modified Au(111). Experimental results show that a small surface coverage of Ag adatoms ($0.10 < \theta_{Ag} < 0.4$) is enough to increase the stability of the thiolate adlayer on the Ag-modified Au(111) surface. This is accompanied by the appearance of multiple peaks during alkanethiol electrodesorption. At higher Ag adatom coverage ($\theta_{Ag} > 0.4$) only the typical electrodesorption peak of alkanethiol from a complete Au(111)−Ag(1 × 1) is observed. The origin of the two peaks in the electrodesorption curves is investigated by DF calculations using periodic slab models for methanethiolate (MT) interacting with different substrate lattices. These calculations indicate that two MT species are laterally bonded to each Ag adatom with rather

[†] Universidad de La Laguna.
[‡] Universidad Nacional de La Plata.
[§] Universitat de Barcelona.

10.1021/jp074698f CCC: $40.75 
Published on Web 03/01/2008

high interaction energy. This implies that MT bonded to Au could be detected only when all Ag adatoms are saturated with the MT species; i.e., for a sufficiently low Ag coverage.

## Experimental Section

Preferred oriented (111) evaporated Au on glass was used as substrate (AF 45 Berliner Glass KG, Germany). After annealing for 10 min with a hydrogen flame these Au substrates exhibit atomically smooth (111) terraces separated by monatomic steps.[19] On an ideal Au(111) plane there are $1.39 \times 10^{15}$ atoms/cm$^2$, and therefore, for this plane, the charge required to form a monolayer of species occupying one site and requiring one electron per site is 222 $\mu$C cm$^{-2}$.[20]

The real surface area of working electrodes was determined by measuring the charge needed to reduce a gold oxide monolayer, which is a two-electron process. This was done by integrating the main cathodic peak in the current−potential curves taken in the supporting electrolyte between 0 V versus a reversible hydrogen electrode (RHE) and the so-called Burshtein minimum.[21−23] The roughness factor average, defined as the ratio of real to geometric surface area, was $1.18 \pm 0.03$. After surface preparation the Au substrates were used as working electrodes for Ag UPD from $5 \times 10^{-4}$ M $Ag_2SO_4$ + 1 M $H_2SO_4$. The amount of electrodeposited Ag was controlled through the applied potential to the Au(111)/electrolyte interface. To this end, the electrodes were immersed in the electrolyte solution under an applied potential $E_a = 0.60$ V versus $Ag^+/Ag$, subjected to a simple scan in the negative potential direction up to a final potential, $E_c$. After a preset Ag surface coverage ($\theta_{Ag}$) was reached, the electrodes were removed from the electrochemical cell under potential control, carefully rinsed with 1 M $H_2SO_4$ and MilliQ water, and finally dried under nitrogen atmosphere. Some of the Ag UPD-covered Au(111) samples were immediately transferred to a ultrahigh vacuum chamber for Auger electron spectroscopy (AES) measurements. Other electrodes were also rinsed with ethanol, dried under $N_2$, and immersed in $5 \times 10^{-5}$ M PT ethanolic solutions for 24 h to yield a complete SAM, and then rinsed carefully with absolute ethanol to remove weakly adsorbed molecules. Some of the PT-covered substrates were then analyzed by AES while other samples were placed in another electrochemical cell containing 0.1 M NaOH to carry out PT electrodesorption experiments and thus determine the electrodesorption potential, $E_p$. Also, the PT-covered samples used for AES analysis were also used as electrodes in electrodesorption experiments.

Electrochemical measurements were made in a conventional three-electrode glass cell at 25 °C using a Pt large area wire as counter electrode. For Ag UPD, a silver wire was used as reference electrode, whereas for PT electrodesorption a saturated calomel electrode (SCE) was employed. Electrodesorption curves were recorded at 0.050 V s$^{-1}$. In all cases the electrolyte solutions were degassed just before taking measurements. The surface coverage of Ag UPD and the surface coverage of chemisorbed PT were calculated from AES data. AES data were recorded using an electron gun operated at 3 keV and 10 mA cm$^{-2}$ by using a single-pass cylindrical mirror analyzer (CMA, Physical Electronics).

## Computational Details and Surface Models

Adsorption of alkanethiols on the Ag-modified Au(111) surfaces was also investigated by means of periodic DF calculations carried out on sufficiently thick slab models. These models are similar to those used in previous work to study the relative stability of various MT phases on Ag(111), including

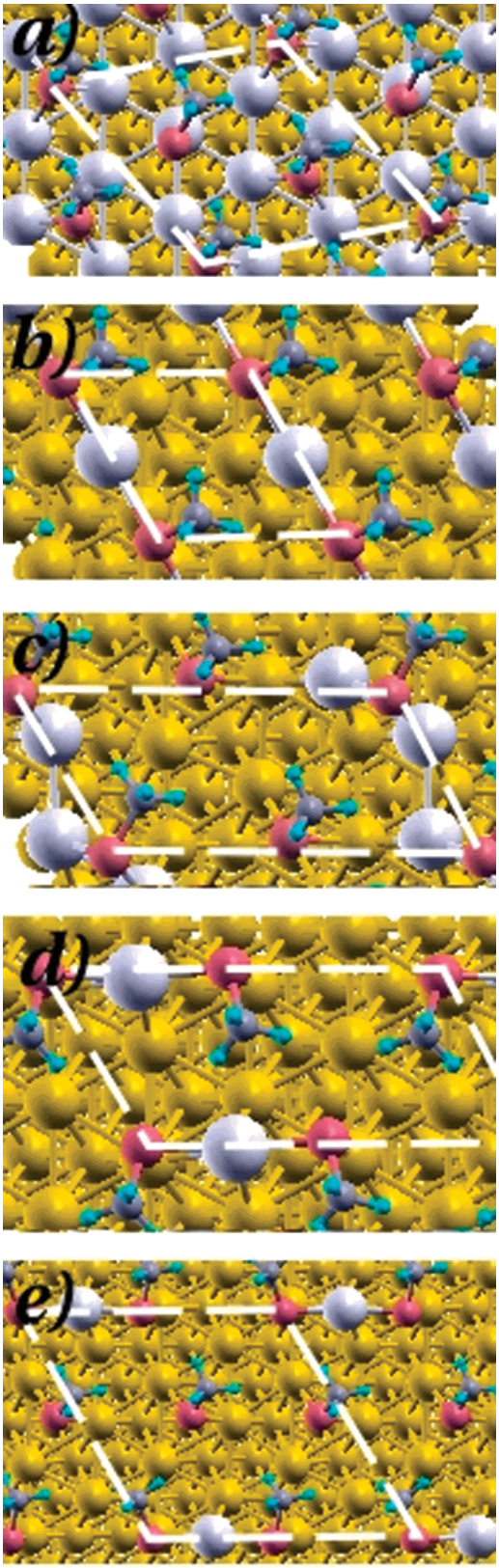


**Figure 1.** Optimized structures for MT on Au(111) surfaces with different amounts of Ag adatoms. (a) $\theta_{Ag} = 1$, MT molecules are directly bonded to fcc, hcp, and top adsorption sites of the silver monolayer; (b) $\theta_{Ag} = 1/3$, MT molecules are bonded to the silver adatom; (c) $\theta_{Ag} = 1/3$ (step Ag), one MT molecule is bonded to the gold substrate, while the other one is bonded to silver; (d) $\theta_{Ag} = 1/6$, MT molecules are bonded at the same time to silver and gold; (e) $\theta_{Ag} = 1/12$, two of the MT molecules are bonded to gold while the other two are bonded to silver and gold.

strongly reconstructed structures.[24] The exchange-correlation energy was expressed within the generalized gradient approximation (GGA) in the formulation of Perdew et al.,[25] commonly referred to as PW91. The valence electron density was expanded in a plane-waves basis set with a cutoff at 420 eV for the kinetic energy. The effect of core electrons in the valence electron density has been taken into account by means of the projector augmented wave (PAW) method[26,27] as implemented by Kresse and Joubert[28] in the VASP code.[29,30] The Brillouin-zone integration was performed using the Monkhorst−Pack method[31] with sufficiently dense *k*-point meshes. Finally, geometry optimization was carried out using a conjugate gradient algorithm and taking advantage that the analytical first derivative of the total energy with respect to nuclear coordinates is implemented in VASP. Systematic convergence checks regarding the number of *k*-points, the energy cutoff, the slab thickness, and vacuum width were carried out for each structural model to ensure that conclusions are derived from essentially converged calculations. Convergence criteria for electronic energy and geometry optimization have been set to $10^{-5}$ and $10^{-4}$ eV, respectively. The calculated lattice parameter for Au ($a = 4.180$ Å) compares reasonably well to the experimental value ($a = 4.078$ Å).

The unreconstructed Au(111) surface was modeled by periodic slabs containing five atomic layers, separated by 10 Å of vacuum. MT was chosen as a model for alkanethiol adsorption. MT species were placed just on one side of the slab, the MT geometry and that of the three topmost atomic layers was fully relaxed, whereas the two Au layers at the bottom of the slab were kept fixed at the calculated Au fcc (face-centered cubic) bulk values. The surface dipole resulting from the above structural arrangement was removed following the standard procedure.[32]

On going from Au(111) to Ag(111) the experimental structure for MT adsorption changes from a Au(111)-($\sqrt{3} \times \sqrt{3}$)R30°−MT ($\theta_{MT} = 0.33$) to a Ag(111)-($\sqrt{7} \times \sqrt{7}$)R19.1°−MT ($\theta_{MT} = 0.43$) pattern. To consistently have also $\theta_{MT} = 0.33$ with different $\theta_{Ag}$ one may either use a large supercell with different amounts of Ag or different supercells. The latter approach permits one to obtain the same results with smaller supercells and a considerable computer time saving. Hence, different unit cell have been used to adjust both the Ag adatom and MT coverages. MT adsorption on Au(111)−Ag(1 × 1) was modeled by a ($\sqrt{7} \times \sqrt{7}$)R19.1° MT unit cell, which is in line with what was observed in STM images obtained for MT on Ag-(111).[33] This surface structure contains the three typical different adsorption sites, namely, hcp (hexagonal close-packed), and fcc hollow and top sites (Figure 1a). Ag adatoms are placed above the fcc sites which, after explicit consideration of several different adsorption sites, are found to be the most favorable ones. Three additional bimetallic Ag on Au(111) surface structures with decreasing Ag coverage ($\theta_{Ag} = 1/3$, 1/6, and 1/12), but keeping the MT coverage ($\theta_{MT} = 0.33$) constant, have been considered. These three bimetallic systems have all a ($\sqrt{3} \times \sqrt{3}$)R30°−MT pattern. In these structures, Ag adatoms are also placed above fcc sites of the Au(111) surface. Accordingly, Au(111)-($\sqrt{3} \times \sqrt{3}$)R30°−Ag, Au(111)-($2\sqrt{3} \times \sqrt{3}$)R30°−Ag, and Au(111)-($2\sqrt{3} \times 2\sqrt{3}$)R30°−Ag unit cells have been used to represent the situation with $\theta_{Ag} = 1/3$, 1/6, and 1/12, respectively (Figure 1, parts b, d, and e).

In all cases the interaction energy ($\epsilon_{int}$) has been calculated by subtracting the energy of the clean surface and the free MT from the energy of surface plus adsorbate using the same unit cell in the three calculations as in eq 1:

$$\epsilon_{int} = \frac{1}{N}[\epsilon(\mathrm{Me})(\mathrm{MT})_N - \epsilon(\mathrm{Me}) - N\epsilon(\mathrm{MT})] \quad (1)$$

where Me stands for the metallic substrate and $N$ is the number of MT species in the unit cell used for each lattice.

The MT electrodesorption potentials from the Ag-containing surface has been estimated assuming that changes in the electrodesorption potential are proportional to changes in the interaction energy ($\Delta\epsilon_{int} \approx \Delta E_p$) and taking $E_p = -0.77$ V for MT electrodesorption from the Au(111)-($\sqrt{3} \times \sqrt{3}$)R30°−MT structure. This value was obtained by extrapolation of the $E_p$ versus $n$ (number of carbon atoms in the alkanethiolate species plot for MT ($n = 1$). The plot $E_p$ versus $n$ was obtained from electrodesorption curves recorded for different ($\sqrt{3} \times \sqrt{3}$)R30° alkanethiolate lattices ($3 \le n \le 12$) under similar experimental conditions as those described in this work.[34]

## Results and Discussion

**1. Electrochemical and AES Results.** The typical voltammogram run at 0.010 V $s^{-1}$ for Ag UPD on the Au(111) substrate is shown in Figure 2a. The Ag electroadsorption stars at 0.60 V, where negative (cathodic) current is related to the following reaction:

$$e + Ag^+ + Au(111) = (Ag)-Au(111) \quad (2)$$

The negative scan exhibits three main, well-defined currents peaks (labeled as CI, CII, CIII in Figure 2a). From atomic force microscopy(AFM)[35] and STM imaging,[36] the peak located at 0.52 V (CI) has been assigned to the formation of a Au(111)-($\sqrt{3} \times \sqrt{3}$)R30°−Ag lattice ($\theta_{Ag} = 1/3$) with the Ag adatoms at fcc hollow sites.[37,38] At slightly more negative potential values a Au(111)-(3 × 3)−4Ag lattice ($\theta_{Ag} = 0.44$) has been observed by in situ AFM[35] and STM.[37] On the other hand, peak CII corresponds to the formation of Au(111)−Ag(1 × 1) lattice. At slightly even more negative values the formation of a second Ag monolayer takes place.[37] The $q$ versus $E$ plot (Figure 2b) is consistent with the voltammetric peak assignment, and it is also in good agreement with data reported by Ogaki and Itaya.[38]

AES spectra corresponding to Ag UPD on Au(111) at different $E_c$ values are shown in Figure 3a. These spectra clearly show that as $E_c$ decreases the Ag signal increases while the Au signal decreases. Therefore, $\theta_{Ag}$ calculated from the Ag/Au signal ratio increases as $E_c$ approaches the $Ag^+/Ag$ couple redox reversible potential in this electrolyte. In Figure 3b, the coverage calculated from our AES data are compared with data obtained by other authors from AES[39,40] and X-ray photoelectron spectroscopy (XPS).[41] It is quite clear that $\theta_{Ag}$ moves from $\theta_{Ag} \sim 0$ at $E_c = 0.600$ V to $\theta_{Ag} = 1.0$ at $E_c = 0.050$ V. We have taken advantage of the results above to prepare Au(111) substrates with different $\theta_{Ag}$ values for thiolate adsorption. This is achieved by holding the applied potential at preset values indicated by vertical arrows in Figure 2a. We have selected $E_c = 0.575$, $E_c = 0.525$, $E_c = 0.500$, and $E_c = 0.050$ V corresponding to $\theta_{Ag} \sim 0.15$, $\theta_{Ag} \sim 0.38$, $\theta_{Ag} \sim 0.60$, and $\theta_{Ag} \sim 1.0$, respectively. As mentioned above the surface coverage $\theta_{Ag} \sim 1.0$ and $\theta_{Ag} \sim 0.38$ can be directly associated with the experimentally observed Au(111)−Ag(1 × 1) and Au(111)-($\sqrt{3} \times \sqrt{3}$)R30°−Ag lattices. The $\theta_{Ag} \sim 0.15$ can be related to more diluted adsorbate surface structures, where we expect that both Ag and Au sites are available for thiolate adsorption. We have also included $E_c = 0.500$ V with $\theta_{Ag} \sim 0.6$ to test the reverse situation, i.e., an excess of silver adatoms relative to the PT adsorbates.

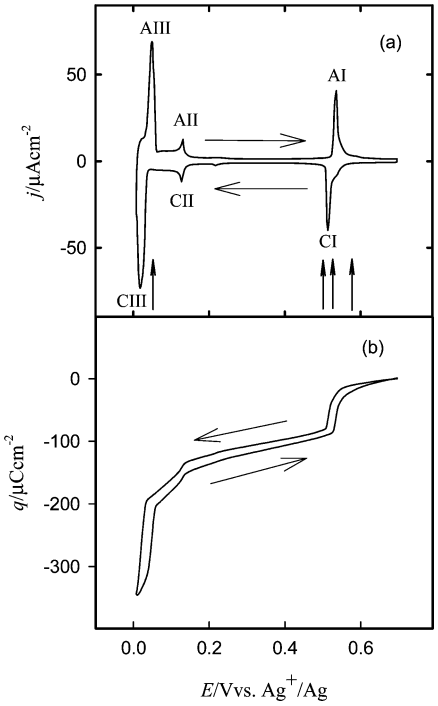


**Figure 2.** (a) Typical $j$ vs $E$ profile for the Au(111) substrate in $5 \times 10^{-4}$ M $Ag_2SO_4 + 1$ M $H_2SO_4$ recorded at a scan rate of $\upsilon = 0.01$ V $s^{-1}$ between $E_a = 0.70$ V and $E_c = 0.005$ V). The typical reversible peaks related to the UPD of two Ag monolayers are shown. (b) Charge density, $q$, vs $E$ plot.

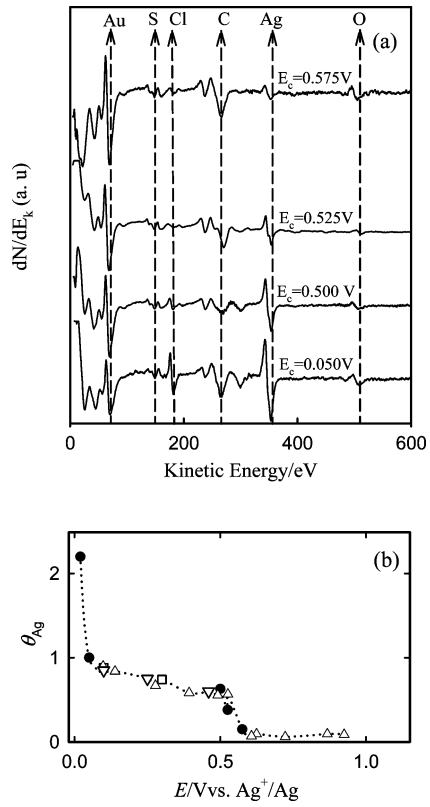


**Figure 3.** (a) Broad AES spectra for the Au(111) substrate voltammetrically cycled in 1 M $H_2SO4$ between $E_a = 0.70$ V and different emersion potentials, $E_c$. (b) Coverage−potential plot of silver adsorbed on the Au(111) surface. Our results are shown as circles, and data obtained by other authors are shown as up triangles (ref 39), squares (ref 40), and down triangles (ref 41, XPS data).

After polarization, the samples were then immediately rinsed with 1 M $H_2SO_4$, MilliQ water, and absolute ethanol, and finally, immersed in a diluted PT-containing ethanolic solution for 24 h in order to adsorb PT. The AES data for the different Ag-modified Au(111) surfaces after PT SAM formation are shown in Figure 4. Comparison of these spectra to those shown in Figure 3a provides strong evidence that PT adsorption did not alter the sample's Ag content. In fact, as $E_c$ decreases from $E_c = 0.525-0.050$ V, the Ag signal increases, the Au signal decreases, and the S signal arising from adsorbed PT is always observed, irrespective of the surface composition. The relatively constant S/C ratio observed for the samples also indicates that now the C signal arises from the hydrocarbon chains of the adsorbed alkanethiolates.

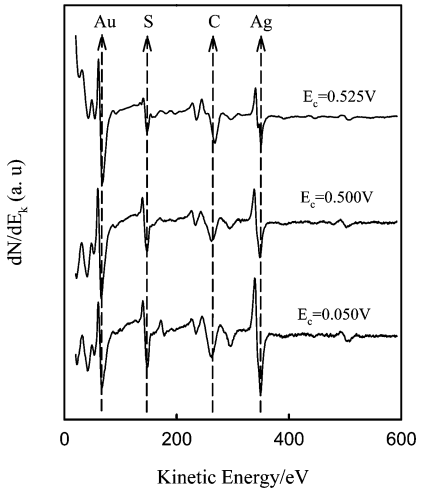


**Figure 4.** AES spectra for propanethiolate SAMs on silver-modified Au(111) substrates. The emersion potentials are indicated.

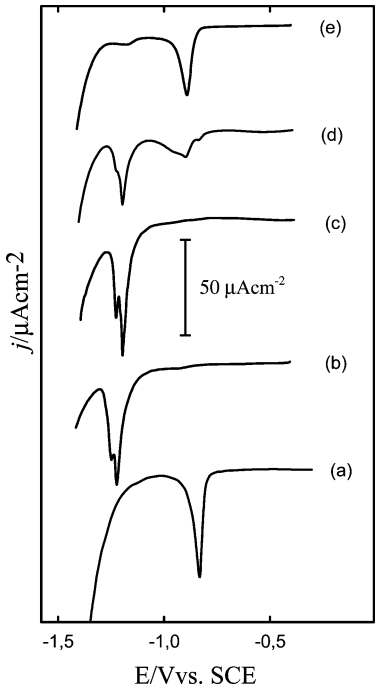


**Figure 5.** Cathodic polarization curves recorded in 0.1 M NaOH at 0.050 V $s^{-1}$ for propanethiolate SAMs on (a) Au(111) and (b−e) Ag-modified Au(111) surfaces with different $\theta_{Ag}$. (b) Ag(1 × 1)−Au(111) (emersion potential $E_c = 0.050$ V in Figure 2a, $\theta_{Ag} \sim 1$), (c) $E_c = 0.500$ V ($\theta_{Ag} \sim 0.6$), (d) $E_c = 0.525$ V ($\theta_{Ag} \sim 0.38$), and (e) $E_c = 0.575$ V ($\theta_{Ag} \sim 0.15$).

Figure 5a displays a typical electrodesorption curve recorded for a PT-covered Au electrode ($\theta_{Ag} = 0$). The PT monolayer desorption occurs at $E_p = -0.83$ V versus SCE where a sharp peak appears preceding the hydrogen evolution reaction (HER).

The amount of charge related to PT electrodesorption is $q_{PT} = 0.071 \pm 0.005$ mC cm$^{-2}$, a quantity close to 0.074 mC cm$^{-2}$, the expected charge for a Au(111)-($\sqrt{3} \times \sqrt{3}$)R30°−PT lattice, corresponding to $7.70 \times 10^{-10}$ mol cm$^{-2}$ for a one-electron process and $\theta_{PT} = 1/3$. Figure 5b shows PT electrodesorption from a Au(111)−Ag(1 × 1) surface ($E_c = 0.05$ V in Figure 2a, $\theta_{Ag} = 1$). The reductive desorption of the PT SAM can be observed as a pronounced current peak at −1.19 V with a smaller peak at a more negative potential.[42] A similar behavior was also observed for hexanethiol SAMs on silver UPD-modified Au(111) electrodes.[43] The amount of charge of both features yields 0.080 ± 0.005 mC cm$^{-2}$ leading to a thiol coverage $\theta_{PT} = 0.36 \pm 0.03$ close to $\theta_{PT} = 0.43$ expected for the ($\sqrt{7} \times \sqrt{7}$)R19° structure. The smaller value for PT arises from the fact that for alkanethiols larger than methanethiol the thiol−thiol distance is 0.48 nm rather than 0.44 nm leading to a slightly distorted ($\sqrt{7} \times \sqrt{7}$)R19°.[42] It is interesting to note that in the case of PT adsorbed on Au(111)−Ag(1 × 1) surfaces, the peak potential is 0.36 V more negative than that corresponding to the Au(111) surface (Figure 5a) and also 0.07 V more negative than that observed from a Ag(111) single-crystal surfaces.[44] This clearly indicates some effect of the Ag UPD layer on stabilizing alkanethiolate SAMs.[42] The electrodesorption curve for PT from a Ag-modified Au(111) surface (Figure 5c) with $\theta_{Ag} \approx 0.60$ ($E_c = 0.50$ V in Figure 2a) is essentially the same shown for $\theta_{Ag} = 1.0$. In fact, within the experimental errors of our measurements, $E_p$ and $q_{PT}$ remain unaltered. This means that PT is preferentially bonded to Ag and that the underlying Au sites play no significant role in the alkanethiol adsorption.[42] Furthermore, the electrodesorption curve for $\theta_{Ag} \approx 0.60$ (Figure 5c) is qualitatively similar to that reported for ethanethiol and octanethiol SAMs on Ag−Au(111) alloy surfaces having a Ag/Au mol ratio of 0.64.[45] Note that no segregation into Ag and Au domains, by displacement of Ag adatoms by the PT species, seems to take place because in this case a detectable peak at around −0.83 V, corresponding to PT desorption from Au(111), should be also observed in the electrodesorption curve.

For $\theta_{Ag} \approx 0.38$ (Figure 5d), $E_c = 0.525$ V in Figure 2a, the situation is, in principle, similar than that observed for $\theta_{Ag} \approx 0.6$ with a main peak at −1.2 V. However, in this case a small peak centered at $E = -0.90$ V and an even smaller one at $E = -0.95$ V are observed. The first conclusion that can be drawn from these results is that no segregation into Ag (islands) and Au domains occurs during PT adsorption even at a relatively low Ag coverage. The second one is that a small quantity of PT is adsorbed on Au sites. However, these sites are now mixed sites in the sense that these are influenced by both Ag adatoms and substrate Au atoms as $E_p = -0.90$ V. In order to identify these sites we have further lowered the Ag adatoms surface coverage to $\theta_{Ag} \approx 0.15$ ($E_c = 0.575$ V in Figure 2a). Although traces of PT bonded to Ag adatoms remain detectable at −1.2 V (Figure 5e), most of the PT is desorbed at $E_p = -0.90$ V. In fact the second mixed state with $E_p = -0.95$ V completely disappears. On the other hand, despite the small number of Ag adatoms present on the Au(111) surface the PT electrodesorption peak is always more negative (≈0.1 V) than that observed for PT on Au(111). Also in this case, there is no evidence of significant phase segregation.

**2. Model Calculations Results.** In order to have a microscopic picture of the effect of Ag adatoms on the adsorption of alkanethiols on Au(111), the adsorption of MT was studied by means of periodic DF calculations, as described in the previous sections. Let us start the discussion by commenting on the Ag surface structures used for Ag adsorption in our DF calculations. Although the Au(111)-($\sqrt{3} \times \sqrt{3}$)R30°−Ag and Au(111)−Ag-(1 × 1) lattices are completely justified by the experimental scanning probe microscopies (SPM) and electrochemical data,[35,37−39] the Ag surface structures related to $\theta_{Ag} < 0.33$ are, in fact, hypothetical lattices. In these cases it is not possible to reasonably associate a model structure to the experimental situation because AES gives only average information about the surface composition, and Ag adatoms are topographically indistinguishable from the substrate by SPM analysis. However, considering that Ag and Au have almost the same atomic radii and lattice parameter in the metallic state and that Ag deposition currently forms commensurate adlattices on Au(111) it is plausible to propose commensurate lattices for the lower surface coverage. Finally, the electrodesorption curve for PT adsorbed on the Ag-modified substrate with $\theta_{Ag} \approx 0.15$ ($E_c = 0.575$ V in Figure 2a) does not show strong evidence of surface segregation of silver adatoms. This behavior is a direct experimental indication which supports the proposed structure.

**TABLE 1: Calculated Average Interaction Energy Per MT Molecule in the Unit Cell ($\epsilon_{int}$) and Calculated Electrodesorption Peak Potential ($E_p$) for MT on Several Models of the Modified Ag Modified Au(111) Surface Assuming a Value of −0.77 for MT on a Au(111) Surface[a]**

| Ag coverage ($\theta_{Ag}$) | thiolate unit cell | $N_{MT}$ | $\epsilon_{int}$/eV | $E_p$/V |
|---|---|---|---|---|
| 1 | ($\sqrt{7} \times \sqrt{7}$)R19.1° | 3 | −1.92 | −1.11 |
| 1/3 | ($\sqrt{3} \times \sqrt{3}$)R30° | 1 | −1.95 | −1.14 |
| | ($2\sqrt{3} \times \sqrt{3}$)R30° | 2 | −2.03 | −1.22 |
| 1/6 | ($2\sqrt{3} \times \sqrt{3}$)R30° | 2 | −1.96 | −1.15 |
| 1/12 | ($2\sqrt{3} \times 2\sqrt{3}$)R30° | 4 | −1.93 | −1.12 |
| 0 | ($\sqrt{3} \times \sqrt{3}$)R30° | 1 | −1.58 | −0.77 |

[a] $\theta_{Ag}$ indicates the Ag coverage, thiolate unit cell indicates the different structural models used which are also displayed in Figure 1, and $N_{MT}$ indicates the number of MT molecules in the corresponding unit cell.

For each one of the different surface structures considered in our DF study, represented by its corresponding unit cell, several thiol adsorption sites were investigated. Notice that the number of MT species varies with the unit cell and that these can occupy different surface sites (Figure 1). Average interaction energies for the different surface structures are collected in Table 1. Indeed, the calculated interaction energies values are of the order of those estimated by thermal-programmed desorption for small-chain alkanethiols on Ag(111).[46]

In agreement with our experimental and previous theoretical results,[42] MT adsorption on Ag atoms is favored with respect to adsorption on the unreconstructed Au(111) surface by ∼0.3 eV (Table 1). Notice that this is precisely in agreement with the experimental finding from the electrodesorption measurements. In addition, the interaction energy on Ag-modified Au-(111) does not significantly change with respect to Ag coverage. This is a strong indication that MT adsorption on Au will only occur when there will be no free Ag adatoms available in the Au surface. In the case of $\theta_{Ag} = 1/12$ coverage, a combination of sites exist where two MT molecules are adsorbed on Ag sites and two on Au(111). This structure provides an explanation for the two peaks present in the reductive desorption curve (Figure 5). One peak would correspond to desorption of thiolates bonded to Ag adatoms and the other one to desorption of thiolates bonded to the Au(111) surface (Table 1). Note that for $\theta_{Ag} = 0.38$ the experimental desorption curve reveals some amount of MT bonded to Au sites. We speculate that this surface coverage involves some amount of Ag decorating Au steps. Therefore, the $\theta_{Ag}$ value on terraces could be smaller with some

thiolates bonded to Au atoms. We have simulated this situation in DF calculations using a Au(111)-($2\sqrt{3} \times \sqrt{3}$)R30°−Ag lattice (Figure 1c). Again, we found an interaction energy similar to that obtained for the other Ag adatoms containing Au(111) surfaces. Obviously, in this case, some thiolates remain adsorbed on the Au(111) surface at the fcc-bridge sites. We conclude that in the real UPD Ag-modified Au(111) system a fraction of Ag is adsorbed at step edges so that the effective surface coverage on the Au(111) terraces is lower than expected.

The intrinsic effect of Ag adatoms can be differentiated from the structural effect by comparing to a model system where Ag adatoms are replaced by Au adatoms. Hence, we have calculated $\epsilon_{int}$ for MT adsorption on such Au on Au(111) surface with 1/3 coverage of Au adatoms. After geometry optimization, we also observe that MT molecules are laterally bonded to the Au adatom. In this case we obtain $\epsilon_{int} = -2.05$ eV. Therefore, on the basis of the similar adsorption energies for MT on Ag or Au adatoms, one may expect similar electrodesorption peak $E_p$ values for the ($\sqrt{3} \times \sqrt{3}$)R30°−MT lattice desorption from 1/3 adatom coverage either Au on Au(111) or Ag on Au(111). However, from the fact that experimental electrodesorption for the ($\sqrt{3} \times \sqrt{3}$)R30°−PT lattice on Au(111) takes place at more positive energies (≈0.3 eV) than that corresponding to 1/3 Ag-adatom-modified surface (Figure 5) one concludes that the ($\sqrt{3} \times \sqrt{3}$)R30° alkanethiolate lattice on Au does not involves any marked adatom reconstruction.

## Conclusions

The adsorption of alkanethiolates on Au(111) surfaces containing different amounts of Ag adatoms has been experimentally and theoretically investigated. Electrodesorption experiments show that thiol desorption from the UPD Ag-modified Au(111) surface requires potentials shifted 0.36 eV in the negative direction with respect to the value corresponding to the same thiol from Au(111) surfaces. Using periodic DF calculations on several different slab models containing different coverages of Ag adatoms on Au(111) we found that alkanethiolates prefer to be laterally adsorbed to Ag adatoms. In particular, the interaction energy to the Ag adatoms is about 0.3 eV larger than that corresponding to the same thiolate on the Au(111) surface, in good agreement with the electrodesorption measurements. Hence, one can conclude that thiolate adsorbed on Au is observed only when the Ag adatom density is small enough.

The preferential adsorption of thiolate for the adatom site is also found for a surface model containing Au adatoms on Au(111) and with a similar gain in interaction energy (∼0.3 eV) on Au adatoms related sites relative to adsorption on the unreconstructed Au(111). This together with the fact that electrodesoption curves for alkanethiolates adsorbed on Au(111) do not show the shift observed for the modified Ag on Au(111) surface leads us to conclude that, under present experimental conditions, the Au(111) surface does not exhibit a significant amount of Au adatoms. This casts reasonable doubts on the generality of the adatom reconstruction models proposed for thiolate on Au(111).[15,17]

**Acknowledgment.** S.G. and D.T. are grateful to the Universitat de Barcelona for a predoctoral fellowship. Financial support has been provided by the Spanish Ministry of Education and Science (Projects MAT2006-14274-C02-01, CTQ2005-08459-CO2-01, CTQ2005-03222/BQU, and UNBA05-33-001), Argentine Agencia Nacional de Promoción Científica y Tecnológica (PICT 02-11111, PICT 05-32980), the National University of La Plata and CONICET (Argentina), and in part, by Generalitat de Catalunya (Projects 2005SGR-00697, 2005 PEIR 0051/69, and Distinció Gen-Cat granted to F.I.) and Gobierno Autónomo de Canarias (Project EQU 2006/027). The authors thankfully acknowledge the computer resources, technical expertise, and assistance provided by the Barcelona Supercomputing Center.

## References and Notes

(1) Schreiber, F. *Prog. Surf. Sci*. **2000**, *65*, 151 and references therein.
(2) (a) Ulman, A. *Chem. Rev.* **1996**, *96*, 1533. (b) Ulman, A. *An Introduction to Ultrathin Organic Films: from Langmuir−Blodgett to Self-Assembly*; Academic Press: Boston, 1991.
(3) Schreiber, F. *J. Phys.: Condens. Matter* **2004**, *16*, R881.
(4) Gates, B. D.; Xu, Q.; Stewart, M.; Ryan, D.; Willson, C. G.; Whitesides, G. M. *Chem. Rev.* **2005**, *105*, 1171.
(5) Haag, R.; Rampi, A. M.; Holmlin, R. E.; Whitesides, G. M. *J. Am. Chem. Soc.* **1999**, *121*, 7895.
(6) Timp, G. *Nanotechnology*; Springer-Verlag: New York, 1999.
(7) (a) Xia, Y.; Rogers, J. A.; Paul, K. E.; Whitesides, G. M. *Chem. Rev.* **1999**, *99*, 1823. (b) Schilardi, P. L.; Azzaroni, O.; Salvarezza, R. C. *Langmuir* **2001**, *17*, 2747.
(8) Finklea, H.O. In *Encyclopedia of Analytical Chemistry: Applications, Theory and Instrumentation*; Meyers, R., Ed.; John Wiley & Sons: Chichester, U.K., 2000.
(9) (a) Anselmetti, D.; Baratoff, A.; Guntherodt, H. J.; Delamarche, E.; Michel, B.; Gerber, Ch.; Kang, H.; Wolf, H.; Ringsdorf, H. *Europhys. Lett*. **1994**, *27*, 365. (b) Terán, F. T.; Vela, M. E.; Salvarezza, R. C.; Arvia, A. J. *J. Chem. Phys*. **1998**, *109*, 5703. (c) Vericat, C.; Vela, M. E.; Salvarezza, R. C. *Phys. Chem. Chem. Phys.* **2005**, *7*, 3258.
(10) Torrelles, X.; Vericat, C.; Vela, M. E.; Fonticelli, M. H.; Daza Millone, M. A.; Felici, R.; Lee, T.-L.; Zegenhagen, J.; Muñoz, G.; Martín-Gago, J. A.; Salvarezza, R. C. *J. Phys. Chem. B* **2006**, *110*, 5586.
(11) Roper, M. G.; Skegg, M. P.; Fisher, C. J.; Lee, J. J.; Woodruff, D. P.; Jones, R. G. *Chem. Phys. Lett.* **2004**, *389*, 87.
(12) Kondoh, H.; Iwasaki, M.; Shimada, T.; Amemiya, K.; Yokoyama, T.; Ohta, T.; Shimomura, M.; Kono, S. *Phys. Rev. Lett.* **2003**, *90*, 066102.
(13) Akinaga, Y.; Najajima, T.; Hirao, K. *J. Chem. Phys*. **2001**, *114*, 8555.
(14) Morikawa, Y.; Hayashi, T.; Liew, C. C.; Nozoye, H. *Surf. Sci.* **2002**, *46*, 507.
(15) Yu, M.; Bovet, N.; Satterley, C. J.; Bengio, S.; Lovelock, K. R. J.; Milligan, P. K.; Jones, R. G.; Woodruff, D. P.; Dhanak, V. *Phys. Rev. Lett.* **2006**, *97*, 166102.
(16) Shimada, T.; Kondoh, H.; Nakai, I.; Nagasaka, M.; Yokota, R.; Amemiya, K.; Ohta, T. *Chem. Phys. Lett.* **2005**, *406*, 232.
(17) Mazzarello, R.; Cossaro, A.; Verdini, A.; Rousseau, R.; Casalis, L.; Danisman, M. F.; Floreano, L.; Scandolo, S.; Morgante, A.; Scoles, G. *Phys. Rev. Lett.* **2007**, *98*, 016102.
(18) (a) Maksymovych, P.; Sorescu, D. C.; Yates, J. T., Jr. *Phys. Rev. Lett.* **2006**, *97*, 146103. (b) Maksymovych, P.; Sorescu, D. C.; Yates, J. T., Jr. *J. Phys. Chem. B* **2006**, *110*, 21161.
(19) Vericat, C.; Vela, M. E.; Andreasen, G.; Salvarezza, R. C.; Vázquez, L.; Martín-Gago, J. A. *Langmuir* **2001**, *17*, 4919.
(20) Angerstein-Kozlowska, H.; Conway, B. E.; Hamelin, A.; Stoicoviciu, L. *J. Electroanal. Chem.* **1987**, *228*, 429.
(21) Michri, A. A.; Pshchenichnikov, A. G.; Burshtein, R. Kh. *Sov. Electrochem.* **1972**, *8*, 351.
(22) Hamelin, A. *J. Electroanal. Chem.* **1996**, *407*, 1.
(23) Trasatti, S.; Petrii, O. A. *Pure Appl. Chem.* **1991**, *63* (5), 711.
(24) Torres, D.; Carro, P.; Salvarezza, R. C.; Illas, F. *Phys. Rev. Lett.* **2006**, *97*, 226103.
(25) Perdew, J. P.; Chevary, J. A.; Vosko, S. H.; Jackson, K. A.; Pederson, M. R.; Singh, D. J.; Fiolhais, C. *Phys. Rev. B* **1991**, *46*, 6671.
(26) Blöchl, P. E. *Phys. Rev. B* **1994**, *50*, 17953.
(27) Blöchl, P. E.; Margl, P.; Schwarz, K. Ab Initio Molecular Dynamics with the Projector Augmented Wave Method. In *Chemical Application of Density-Functional Theory*; Laird, B. B., Ross, R. B., Ziegler, T., Eds.; American Chemical Society: Washington, DC, 1996.
(28) Kresse, G.; Joubert, D. *Phys. Rev. B* **1998**, *59*, 1758.
(29) Kresse, G.; Furthmüller, J. *Phys. Rev. B* **1996**, *54*, 11169.
(30) Kresse, G.; Hafner, J. *Phys. Rev. B* **1993**, *47*, 558.
(31) Monkhorst, H. J.; Pack, J. D. *Phys. Rev. B* **1976**, *13*, 5188.
(32) Kresse, G.; Furthmüller, J. *J. Comput. Mater. Sci.* **1996**, *6*, 15.
(33) Yu, M.; Driver, S. M.; Woodruff, D. P. *Langmuir* **2005**, *21*, 728.
(34) Vela, M. E.; Martin, H.; Vericat, C.; Andreasen, G.; Hernández Creus, A.; Salvarezza, R. C. *J. Phys. Chem. B* **2000**, *104*, 11878.
(35) Chen, C. H.; Vesecky, S. M.; Gerwirth, A. A. *J. Am. Chem. Soc.* **1992**, *114*, 451.

(36) Borissov, D.; Aravinda, C. L.; Freyland, W. *J. Phys. Chem. B* **2005**, *109*, 11606.
(37) Esplandiu, M. J.; Schneeweiss, M. A.; Kolb, D. M. *Phys. Chem. Chem. Phys.* **1999**, *1*, 4847.
(38) Ogaki, K.; Itaya, K. *Electrochim. Acta* **1995**, *40*, 1249.
(39) Mrozek, P.; Sung, Y. E.; Han, M.; Gamboa-Adelco, M.; Wieckowski, A.; Chen, C. H.; Gerwirth, A. A. *Electrochim. Acta* **1995**, *40*, 17.
(40) Rooryck, V.; Reniers, F.; Buess-Herman, C.; Attard, G. A.; Yang, X. *J. Electroanal. Chem.* **2000**, *482*, 93.
(41) Jennings, G. K.; Laibinis, P. E. *Langmuir* **1996**, *12*, 6173.
(42) Fonticelli, M.; Azzaroni, O.; Benitez, G.; Martins, M. E.; Carro, P.; Salvarezza, R. C. *J. Phys. Chem. B* **2004**, *108*, 1898.
(43) Esplandiu, M. J.; Hagenström, H. *Solid State Ionics* **2002**, *150*, 39.
(44) (a) Hatchett, D. W.; Stevenson, K. J.; Lacy, W. B.; Harris, J. M.; White, H. S. *J. Am. Chem. Soc*. **1997** *119*, 6596. (b) Hatchett, D. W.; Uibel, R. H.; Stevenson, K. J.; Harris, J. M.; White, H. S. *J. Am. Chem. Soc*. **1998**, *120*, 1062. (c) Mohtat, N.; Byloos, M.; Soucy, M.; Morin, S.; Morin, M. *J. Electroanal. Chem*. **2000**, *484*, 120. (d) Azzaroni, O.; Vela, M. E.; Andreasen, G.; Carro, P.; Salvarezza, R. C. *J. Phys. Chem. B* **2002**, *106*, 122671.
(45) Kawazaki, M.; Iino, M. *J. Phys. Chem. B* **2006**, *110*, 21124.
(46) Rodriguez, L. M.; Gayone, J. E.; Sanchez, E. A.; Grizzi, O.; Blum, B.; Salvarezza, R. C. *J. Phys. Chem. B* **2006**, *110*, 7095.